ACS OMEGA

Open Access

http://pubs.acs.org/journal/acsodf

Article

The Relationship between the Electronic State of Pt in Pt-Based Nanoparticle Catalysts and Their Electrochemical Catalytic Activity in the Oxidation of Small Organic Compounds

Tamaki Matsumura, Mika Fukunishi, and Futoshi Matsumoto*

Cite This: *ACS Omega* 2025, 10, 10060−10070

Read Online

ACCESS | Metrics & More | Article Recommendations | Supporting Information

ABSTRACT: To examine the relationship between the electronic state of platinum (Pt) in Pt-based nanoparticle (NP) catalysts and their catalytic activities in the electrochemical oxidation of methanol (MeOH) and ethanol (EtOH) in alkaline aqueous solutions, Pt-based NP catalysts were synthesized; their electrocatalytic activities were evaluated by rotating electrode techniques; and the electronic state of Pt in Pt-based catalyst surfaces was analyzed *via* X-ray photoelectron spectroscopy (XPS) and X-ray absorption spectroscopy (XAS). Finally, plots of the electrocatalytic activity *vs* electronic state of the Pt atoms on the catalyst surface were obtained. The plots exhibited a so-called volcano-type correlation, indicating that there is an optimum electronic state of Pt atoms on the catalyst surface for maximizing the MeOH and EtOH oxidation activities. In addition, the existence of the optimum electronic state was confirmed with adatom-modified Pt electrodes with Pb, Bi, In, Co, and Cu.

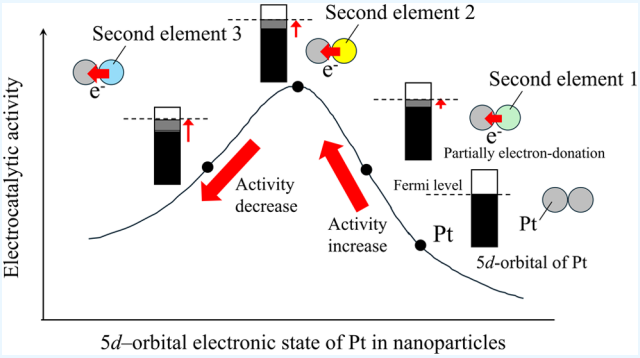

INTRODUCTION

Polymer−electrolyte membrane fuel cells (PEMFCs), in which polymer membranes work as ion conductors between the anode and cathode, are attracting increasing interest as portable energy sources for electric vehicles and mobile electronics and stationary energy sources at operation temperatures ranging from ordinary temperatures to 100 °C.[1,2] Fuels such as hydrogen (H_2), methanol (CH_3OH, MeOH),[3] ethanol (C_2H_5OH, EtOH),[4] formic acid (HCOOH),[5] and dimethyl ether (CH_3OCH_3)[6] are oxidized on anode catalyst surfaces to produce protons (H^+) and electrons (e^-), which are transferred through the H^+-conductive polymer−electrolyte membrane and through the external circuit to the cathode, respectively. Compared with fuel cells using H_2 fuel, direct-oxidation fuel cells (DOFCs), in which carbon-containing fuels such as MeOH, EtOH, HCOOH, and CH_3OCH_3 are oxidized on anodes, have several advantages, such as the elimination of a reformer for the conversion of carbon-containing fuels to H_2 and a humidification and thermal management system.[7] Therefore, DOFCs are still being researched and developed.[8] One hindrance to the development of DOFCs is alcohol crossover behavior, in which alcohols supplied as fuels to anodes permeate through polymer−electrolyte membranes to cathodes, which impedes oxygen reduction at the cathode and decreases the power generation efficiency.[9] To reduce alcohol crossover, alkaline polymer electrolytes in which hydrogen oxide (OH^-) is transferred from the cathode to the anode have been used.[10] An additional advantage of changing from H^+- to OH^--conductive polymer−electrolyte membranes in DOFCs is the expansion of the selection range of electrocatalysts for anodes and cathodes. Although platinum (Pt)- and palladium (Pd)-based catalysts have been used for anodes in H^+-conductive polymer−electrolyte membranes,[8] OH^--conductive polymer−electrolyte membranes allow the use of non-noble metal catalysts.[11] The development of anode catalysts for alcohol oxidation in alkaline aqueous solutions is still being examined. The authors reported that PtPb and PtBi intermetallic compounds exhibited high and stable activity for MeOH and EtOH in alkaline aqueous solutions on the basis of examinations of various Pt-based intermetallic compounds.[12] The results revealed that the PtPb intermetallic compound exhibited the highest oxidation activity for MeOH and EtOH, and the PtBi intermetallic compound had the highest durability among the Pt-based intermetallic compounds examined in the study. The electrocatalytic activity strongly depended on the type of second element in the Pt-

Received: September 12, 2024
Revised: February 27, 2025
Accepted: March 4, 2025
Published: March 10, 2025

https://doi.org/10.1021/acsomega.4c08380
ACS Omega 2025, 10, 10060−10070

Table 1. Summary of the Synthesis Conditions for the NPs

sample name	source of the second element in NPs	molar ratio of Pt and the second element in the synthesis solution	synthesis process	reaction temperature (°C)	reaction condition	calcination temperature (°C) and period (min)
(b) $PtRh_{0.5}/CB$	Rhodium(II) acetate dimer	1:1 (Pt/Rh)	microwave polyol process	200	microwave irradiation for 30 min ×1 time	none
(c) PtBi/CB	Bismuth(III) nitrate pentahydrate	1:1	microwave polyol process	265	microwave irradiation for 10 min ×3 times	none
(d) $PtCo_{1.3}/CB$	Cobalt(II) acetate tetrahydrate	1:2	microwave polyol process	265	microwave irradiation for 10 min ×5 times	none
(e) $PtPb_{1.1}/CB$	Lead(II) acetate trihydrate	1:1.5	microwave polyol process	265	microwave irradiation for 5 min ×3 times	none
(f) $PtIn_{1.3}/CB$	Indium(III) nitrate trihydrate	1:1	microwave polyol process	265	microwave irradiation for 30 min ×1 time	none
(g) $PtCu_{1.4}/CB$	Copper(II) chloride	1:1.2	microwave polyol process	265	microwave irradiation for 10 min ×5 times	none
(h) $PtCo_{2.0}/CB$	Cobalt(II) acetate tetrahydrate	1:2.5	microwave polyol process	265	microwave irradiation for 10 min ×5 times	300, 90
(i) $PtSn_{3.1}/CB$	Tin(II) chloride dihydrate	1:2	microwave polyol process	265	microwave irradiation for 30 min ×3 times	none
(j) $PtSn_{3.3}/CB$	Tin(II) chloride dihydrate	1:3	microwave polyol process	265	microwave irradiation for 30 min ×3 times	none
(k) $PtIn_{2.4}/CB$	Indium(III) nitrate trihydrate	1:2	microwave polyol process	265	microwave irradiation for 30 min ×1 time	300, 90
(l) $PtFe_{2.3}/CB$	Iron(III) nitrate nonahydrate	1:3	LiTEBH process	52	stirring for 12 h	500, 90
(m) $PtSb_{1.4}/CB$	Antimony(III) chloride	1:1.3	microwave polyol process	265	microwave irradiation for 10 min ×3 times	none

based intermetallic compounds. In addition, authors and coworkers have reported that the electrocatalytic activity of the oxygen reduction reaction (ORR) can be related to the d-band center of Pt in Pt materials and Pt-based NPs. In short, a so-called volcano-type correlation between the ORR activity and the d-band center was maintained for a series of catalysts prepared in this research.[13,14] To continue this discussion, the volcano-type correlation between the electrocatalytic activity and the d-band center of Pt in catalysts should be investigated in electrochemical reactions other than the ORR. In this study, the electrochemical oxidation of MeOH and EtOH on Pt-based alloy catalysts in alkaline aqueous solution is the targeted reaction for investigations of the volcano-type correlation. To systematically change the values of the d-band center, the type and elemental ratio of the secondary element in the Pt-based NPs were controlled by the conditions used to synthesize the NPs. In addition, the electronic states of Pt were determined by measuring the electronic state of the valence band region of Pt *via* X-ray photoelectron spectroscopy (XPS), and the d-band center values for each sample were evaluated. However, when discussing the electronic state of catalysts, the degree of vacancy in the 5d orbital has been recently measured *via* X-ray absorption spectroscopy (XAS).[15] Therefore, in this study, we also examined Pt-based NP samples by measuring both the d-band center via XPS and the degree of vacancy in the 5d orbital via XAS[15] and confirmed that a similar volcano-shaped relationship was obtained between the degree of vacancy in the 5d orbital obtained *via* XAS measurements and the catalytic activity.

EXPERIMENTAL SECTION

Preparation of Pt-Based NPs. The starting materials and conditions used for the preparation of carbon (carbon black (CB), Vulcan carbon XC-72, and E-TEK)-supported Pt-based NP catalysts are listed in Table 1. Throughout this paper, Pt NP/CB (Pt loading weight percentage: 20%) and 12 Pt-based NP catalyst/CB samples are designated with the notations (a)−(m) in Table 1. Two approaches were taken to synthesize the NPs. The first method is a polyol process. Pt-based NPs were prepared in ethylene glycol, which functions as a solvent and reducing agent for reducing second metal ions under microwave irradiation of the reaction solution. For example, in the preparation of the (e)$PtPb_{1.1}/CB$ catalyst, Pt/CB (0.040 g, Pt: 0.04 mmol) was dispersed and lead(II) acetate ($Pb(CH_3COO)_2$, 0.06 mmol) was dissolved in 50 mL of ethylene glycol (EG). For all of the NP preparations, 50 mL of EG and 0.04 mmol of Pt in the Pt NPs/CB were fixed. The mixture was treated in a flask with reflux at a microwave power of 300 W. A schematic depiction of the polyol process used to prepare Pt-based NPs on CB by reacting second metal ions (M^{n+}) with reducing agents on the Pt surfaces of Pt NP/CB is shown in Figure 1. With this method, there is little difference in the dispersion state of the NPs on the CB between the prepared NPs. The second method is a conventional method in which second metal ions are reduced on the Pt surfaces of Pt NP/CB by the reducing agent lithium triethyl borohydride (LiTEBH) in organic solvents (LiTEBH process). When targeted NPs cannot be synthesized via the microwave polyol process, the LiTEBH process is applied to prepare the Pt-based NPs on CB. In the LiTEBH process, Pt/CB and a second metal source were added to 30 mL of a tetrahydrofuran solvent. A total of

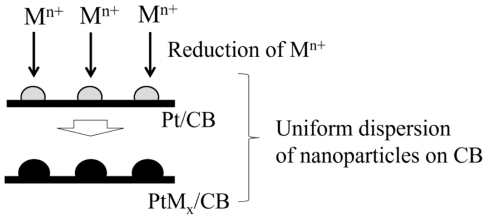

Figure 1. Schematic depiction of the polyol and LiTEBH processes used to prepare Pt-based NPs on CB by reacting second metal ions (M^{n+}) with reducing agents on the Pt NP surfaces of Pt NPs/CB.

https://doi.org/10.1021/acsomega.4c08380
ACS Omega 2025, 10, 10060−10070

0.0308 mmol of Pt was present in the reaction mixture. After thorough stirring, 4 mmol of LiTEBH was added to the reaction mixture and the mixture was subsequently stirred for a set period of time to allow the reaction to proceed at 25 °C.

The first purpose of this study was to compare the oxidation activities of various Pt-based NPs with different d-band centers. For an accurate activity comparison, the synthesis conditions were adjusted so that the number of Pt atoms supported on CB and the average particle size of the NPs could be matched as much as possible. As a result, the average particle size of the NPs was 3.0−4.0 nm, and the loading percentage of Pt in the NP/CB was 15−20 wt %. The average particle size was evaluated with TEM images by measuring the diameter of 50 particles from the TEM images. The atomic percentages of Pt in the NPs and the Pt loading percentages in the NPs/CB were determined via inductively coupled plasma−mass spectrometry (ICP−MS, Agilent, 7700× spectrometer) after dissolving the NPs/CB in aqua regia.

Characterization of Pt-Based NPs. The crystal structure of the Pt NP and Pt-based NPs prepared on CB was evaluated via powder X-ray diffractometry (*p*XRD, RINT-Ultima III; λ = 0.15418 nm, Rigaku) with Cu Kα radiation. The size and distribution of the NPs on CB and the composition of the NPs were analyzed with transmission electron microscopy (TEM) at 200 kV and/or scanning transmission electron microscopy (STEM, JEM-ARM200F, JEOL, Japan) equipped with two aberration correctors (CEOS GmbH) for image- and probe-forming lens systems and an X-ray energy-dispersive spectrometer (JED-2300T, JEOL). The atomic percentages of Pt and secondary elements in an NP on CB were also evaluated via TEM-EDS. In the high-angle annular dark-field (HAADF)-STEM observations, the probe convergence angle and inner angle of the HAADF detector were 29 and greater than 100 mrad, respectively.

Preparation of Catalyst-Coated Electrodes and Electrocatalytic Activity Tests. To prepare the catalyst-coated electrodes, individual catalyst inks were first prepared via the following procedure. 4 mg of the dried NP/CB sample, 3.98 mL of water, 1 mL of isopropyl alcohol, and 20 μL of 5% w/w Nafion solution (EW: 1,100, Aldrich) were mixed and then sonicated in a bath-type ultrasonicator for 15 min. The volume of ink, which was deposited on a glassy carbon (GC) electrode with a diameter of 6 mm, was adjusted to maintain a Pt atom loading weight of 70 μg cm^{-2} on the GC electrodes. That is, considering the amount of catalyst supported on CB and the content of Pt in the NP catalyst, regardless of the type of NP, 70 μg cm^{-2} Pt atoms were supported on the GC electrodes. To deposit the NPs on the GC electrodes, after the ink was deposited on the GC electrode, water and isopropyl alcohol, which are constituents of the ink, were evaporated under vacuum at 60 °C.

Rotating disk electrode voltammograms for alcohol oxidation were measured at a potential scan rate of 10 mV s^{-1} and a rotation rate of 1600 rpm over the potential region between −0.6 and −0.1 V (vs Ag/AgCl (3 M NaCl)) in a 0.1 M sodium hydroxide (NaOH) aqueous solution containing 0.5 M MeOH (or 0.5 M EtOH) under nitrogen (N_2) gas at room temperature (25 ± 0 °C). The background currents, measured in 0.1 M NaOH aqueous solution under the same experimental conditions, were subtracted from the voltammograms. An Ag/AgCl (3 M sodium chloride (NaCl)) reference electrode and a Pt wire counter electrode in which the working and counter electrode components were separated by glass frits and in which the reference electrode was connected through a salt bridge of potassium chloride (KCl) to a 0.1 M $HClO_4$ solution were used.

To calculate the current density of each catalyst for alcohol oxidation with respect to the surface area of GC electrodes. All of the voltammograms were measured via a VMP3 instrument (Bio-Logic Science Instruments, France). The oxidation of formaldehyde and potassium formate (97.0+%) was also investigated under conditions similar to those used in the experiments on the oxidation of MeOH and EtOH. The method for electrochemically evaluating the oxidation potential of carbon monoxide (CO) adsorbed on the catalyst surface is described in the SI.

Determination of the 5d-Band Centers and 5d Orbital Vacancy of Pt in Pt-Based NPs. The d-band center of Pt in the Pt-based NPs, as an index of the electronic state of Pt, was measured *via* X-ray photoelectron spectroscopy (XPS, JP-9010 MC, JEOL) with a Mg Kα X-ray source. All of the XPS spectra were calibrated via the binding energy 1s of the C−C bond in the CB of CB-supported Pt-based NPs. After the baselines of the XPS spectra near the valence band region were subtracted, the values of the d-band centers were evaluated *via* eq 1.[16−18]

$$\text{d-band center} = \int_{x\text{eV}}^{0\text{eV}(E_f)} (\text{binding energy}(E) \times \text{intensity}(E))\text{d}E / \int_{x\text{eV}}^{0\text{eV}(E_f)} \text{intensity}(E)\,\text{d}E \quad (1)$$

where E_f is the Fermi level. The lower limits (x) of integration of eq 1 were varied, depending on the spectrum of the sample. The value of the d-band center is expressed as the energy difference between the average energy of the electrons occupying the d-orbitals and the Fermi level. The calculation of the d-band center value from the obtained spectrum involves removing the baseline from the obtained spectrum and calculating the area of the spectrum after the baseline. Spectral software (SpecSurf (Analysis), JEOL) was used for these two tasks. The same software was also used to determine the bounding energy (d-band center value) that divides the calculated spectrum area in half.

XAS measurements for evaluating the 5d orbital vacancy in Pt on the Pt-based NPs were performed at BL01B1 in SPring-8 (Japan). The XAS signals at the Pt L_3 and L_2 edges are measured. The 5d orbital vacancy was calculated from the obtained spectrum *via* the calculation method proposed by Mansour *et al.*[19] The calculation method was based on the method of Mansour and the calculation method described in detail in the paper by Uchimoto et al.[15,19] The 5d orbital vacancy (h) was evaluated with eqs 2−5.

$$f_D = \frac{\Delta A_3 + 1.11\Delta A_2}{A_{3r} + A_{2r}} \quad (2)$$

$$h = (1.0 + f_D)h_{\text{reference}} \quad (3)$$

$$h_{\text{reference}} = 3.0 \quad (4)$$

$$\Delta A_3 = A_{3s} - A_{3r},\ \Delta A_2 = A_{2s} - A_{2r} \quad (5)$$

where the subscripts s and r refer to the sample and reference sample, respectively. The reference sample was a Pt foil. A_3 and A_2 are the areas between the spectrum and the baseline. Also

https://doi.org/10.1021/acsomega.4c08380
ACS Omega 2025, 10, 10060−10070

when the 5d orbital vacancy in Pt is calculated, the operations of removing baselines from the obtained spectrum and calculating the spectrum areas are required. These two operations were performed using software (Athena, developed by Bruce Ravel[20]) used for general analysis at BL01B1 of SPring-8, where the measurements were performed.

Preparation of Adatom-Modified Pt Electrodes. The electrolyte solutions used for adatom deposition included bismuth nitrate pentahydrate, lead(II) acetate trihydrate (99.0%), cobalt(II) acetate tetrahydrate (99.0+), indium(III) nitrate trihydrate (97.0+%), and copper(II) nitrate trihydrate (99.0−104.0%) salts as the raw materials for adatoms. Before the experiments for MeOH and EtOH oxidation, a Pt rotating disk electrode (6 mmφ) was polished with diamond paste and sonicated in an ultrasonic bath with acetone and water. The electrode potential of the Pt rotating disk electrode was then scanned at 10 mV s^{-1} in a deaerated 0.1 M $HClO_4$ solution between the onset potentials of H_2 and O_2 evolution on the Pt surfaces until well-known cyclic voltammograms characteristic of clean Pt surfaces were obtained. The underpotential deposition (UPD) of metals that were used as second elements of Pt-based NPs from solutions containing their ions in a 0.1 M $HClO_4$ aqueous solution was performed. The adatom-modified Pt electrodes were prepared by scanning the electrode potential from the open-circuit potential of the Pt disk electrode in 0.1 M $HClO_4$ aqueous solution to the adatom potential for second elements under a N_2 atmosphere. The potential sweep was stopped at the potential where the reduction peak for the adatom reaction had ended, and the deposition of the adatom was completed. After rinsing the adatom-modified Pt electrodes with water, the adatom-modified Pt electrodes were transferred for MeOH oxidation to test solutions containing MeOH and NaOH aqueous solutions.[22] In order to preserve the prepared adatom-modified Pt electrodes, the electrodes were quickly washed, and before measuring the voltammogram for the MeOH oxidation reaction during bubbling with N_2 gas, electrode potentials slightly more negative than the open-circuit state was applied to the adatom-modified Pt electrodes, and the potential sweep was started from that electrode potentials. Voltammograms for MeOH oxidation were measured in the solutions.

RESULTS AND DISCUSSION

Characterization of Pt-Based NPs. Figure 2 shows *p*XRD patterns of (a) Pt/CB, (b-m) synthesized CB-supported Pt-based NPs, and (n) CB with standard peak patterns (1−12). The XRD data of the synthesized NP samples do not necessarily match the literature values. The peak patterns were similar to the standard peak patterns, but the peak positions were often slightly different, suggesting that the crystal structure may be distorted.

The ratios of Pt to the second element in the NPs revealed by ICP analysis (these elemental ratios are used to describe the NPs) also differ from the elemental ratio of the standard peak. Although NPs of perfect alloys or intermetallic compounds could not be formed, NPs containing Pt and second elements with various atomic ratios were obtained, so we decided to proceed with the study using these samples. The atomic ratios of Pt and second elements in the Pt-based NPs evaluated *via* ICP−MS and TEM−EDS are summarized in Table 2. A comparison of the values of the atomic ratio, which were obtained *via* ICP−MS and TEM−EDS, revealed that the ratios of the second elements obtained *via* ICP−MS are greater than

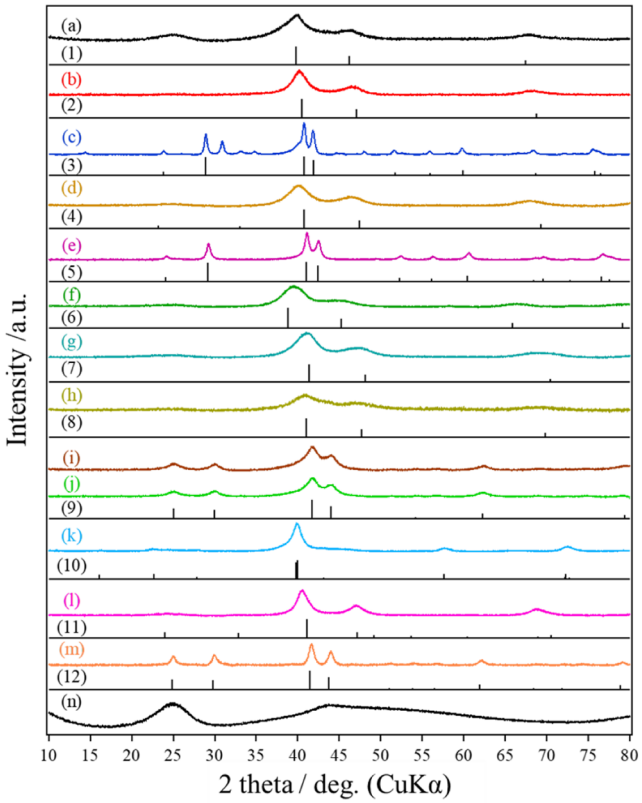

Figure 2. *p*XRD patterns of (a) Pt/CB, (b)$PtRh_{0.5}$/CB, (c) PtBi/CB, (d) $PtCo_{1.3}$/CB, (e) $PtPb_{1.1}$/CB, (f) $PtIn_{1.3}$/CB, (g) $PtCu_{1.4}$/CB, (h) $PtCo_{2.0}$/CB, (i) $PtSn_{3.1}$/CB, (j) $PtSn_{3.3}$/CB, (k) $PtIn_{2.4}$/CB, (l) $PtFe_{2.3}$/CB, (m) $PtSb_{1.4}$/CB, and (n) CB. Theoretical XRD patterns: (1) Pt $Fm\bar{3}m$, (2) PtRh $Fm\bar{3}m$, (3) PtBi $P6_3/mmc$, (4) Pt_3Co $Pm\bar{3}m$, (5) PtPb $P6_3/mmc$, (6) Pt_3In $Pm\bar{3}m$, (7) $Pt_{0.5}Cu_{0.5}$ $Fm\bar{3}m$, (8) $Pt_{0.5}Co_{0.5}$ $Fm\bar{3}m$, (9) PtSn $P6_3/mmc$, (10) Pt_2In_3 $P\bar{3}m1$, (11) PtFe $P4/mmm$, and (12) PtSb $P6_3/mmc$.

Table 2. Summary of the Atomic Ratios of Pt Atoms and the Second Element in the Prepared Pt-Based NPs

	atomic ratio of Pt and the second element in NPs	
sample name	ICP-MS data	TEM-EDS data
(b) PtRh/CB	1.0:0.5	1.00:0.89
(c) PtBi/CB	1.0:1.0	1.00:0.31
(d) PtCo/CB	1.0:1.3	1.00:0.09
(e) PtPb/CB	1.0:1.1	1.00:0.69
(f) PtIn/CB	1.0:1.3	1.00:0.55
(g) PtCu/CB	1.0:1.4	1.00:0.56
(h) PtCo/CB	1.0:2.0	1.00:0.35
PtSn/CB	1.0:3.1	1.00:1.04
PtSn/CB	1.0:3.3	1.00:1.07
PtIn/CB	1.0:2.4	1.00:0.88
PtFe/CB	1.0:2.3	1.00:0.20
PtSb/CB	1.0:1.4	1.00:0.46

those obtained *via* TEM−EDS. The large difference between the values obtained by the ICP−MS and TEM−EDS measurements indicates that a small proportion of the secondary element is deposited as particles singly on the CB surfaces. When the measurements were made with TEM-EDS, it can be considered that elemental analysis is performed within the NPs. In the case of ICP−MS, the entire catalyst is analyzed. When looking at the molar ratio of the second

https://doi.org/10.1021/acsomega.4c08380
ACS Omega 2025, 10, 10060−10070

element to Pt, the ICP results are significantly larger than the TEM-EDS results. Considering the part being analyzed, this difference is thought to indicate the presence of the second element on the CB. Considering the synthesis of the sample used in this study, it is thought that the ions of the second element are reduced on the Pt particles with a reducing agent, but it can be thought that some of them are reduced on the CB to form particles of the second element alone. Therefore, the ICP, which analyzes the entire catalyst, results in a large proportion of the second element. A study using deposits of only second elements on CB prepared separately confirmed that the oxidation reactions of MeOH and EtOH do not proceed on the surface of the deposits of the second element.

To confirm the dispersion of the NPs on the CB and their particle size, TEM images were obtained. Low- and high-resolution TEM images of all of the samples are shown in Figures S1 and S2, respectively. The low- and high-resolution TEM images confirmed that the samples had average diameters of 3.0−4.0 nm. Figure S3 shows the STEM and EDS mapping images of each sample. The average elemental ratios of Pt and the second element in the Pt-based NPs were calculated from these EDS data.

Electrochemical Oxidation of Alcohols with Pt-Based NPs and Their Volcano Plots. Figure 3 shows linear sweep voltammograms for (A) MeOH and (B) EtOH oxidation of the prepared Pt-based NPs. As mentioned above, the current densities were calculated from the GC electrode surface, because the Pt surface on the Pt-based NPs cannot be evaluated. On the Pt-based NPs, reduction and oxidation currents for hydrogen adsorption and desorption cannot be seen clearly due to alloying of second elements to Pt NPs. It is believed that estimating the Pt surface area using the electric charge required for adsorption and oxidation of the monolayer of hydrogen on Pt surface (210 μC cm^{-2})[23] can result in large errors. Therefore, in this study, the amount of Pt element supported on the CB, the diameter of the NPs, and the amount of Pt fixed to the GC electrode were all set to be the same in all samples, allowing a relative comparison of the current densities.

In MeOH oxidation (A), the oxidation current density increases by approximately −0.5 to −0.3 V. Assuming that the onset potential is the voltage at which the current density is 1 mA cm^{-2}, the values of the onset potential and current density of the Pt-based NPs observed at −0.1 V for MeOH and EtOH oxidation were evaluated and are summarized in Tables S1 and S2, respectively. The plots of the onset potential vs current density for (A) MeOH (Figure 4) and (B) EtOH (Figure S4) oxidation via voltammetry are shown. As is generally believed,[24] the plot shows that the smaller the onset potential is, the higher the activity in both oxidation reactions. Therefore, rather than looking at catalytic activity from the onset potential value, which is unclear in its determination (in the case of oxidation reactions, catalytic activity is higher when the onset potential is more negative), catalytic activity can be compared by comparing the oxidation current density values at a certain potential. The linearity of the relationship between the onset potential and the oxidation current density value in Figures 4 and S4 is 0.42 and 0.76 as regression coefficients, respectively. In the case of Figure 4, the data of (m) was deleted for the calculation. Although it cannot be determined with certainty that there is a linear relationship, it is thought that it can be concluded that there is a tendency for the oxidation current value to be high when the onset potential is low. Therefore, it is possible to see the level of catalytic activity depending on the magnitude of the oxidation current at −0.1 V.

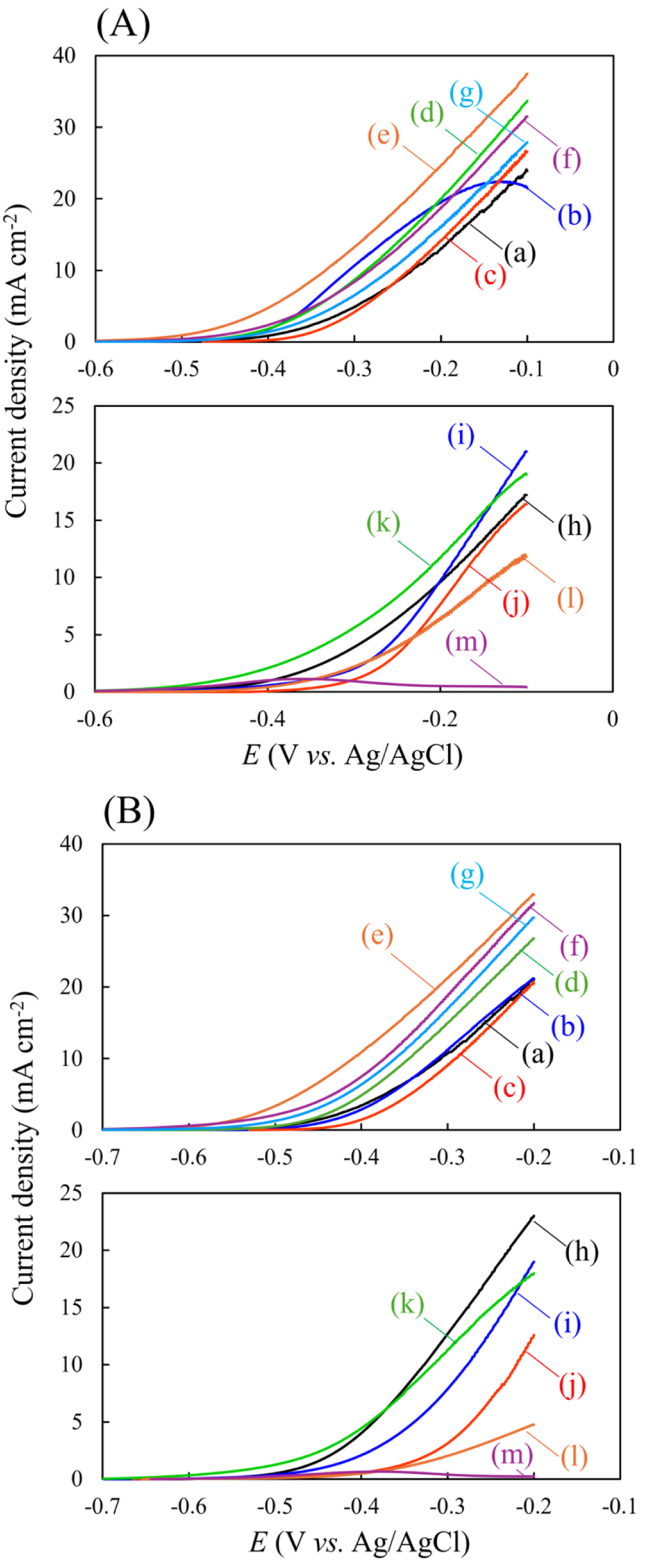

Figure 3. Linear sweep voltammograms for (A) MeOH and (B) EtOH oxidation on (a) Pt/CB and (b−m) Pt-based NPs/CB in N_2-saturated 0.5 M MeOH (or EtOH) and 0.1 M NaOH aqueous solutions at 10 mV s^{-1} and 2000 rpm.

https://doi.org/10.1021/acsomega.4c08380
ACS Omega 2025, 10, 10060−10070

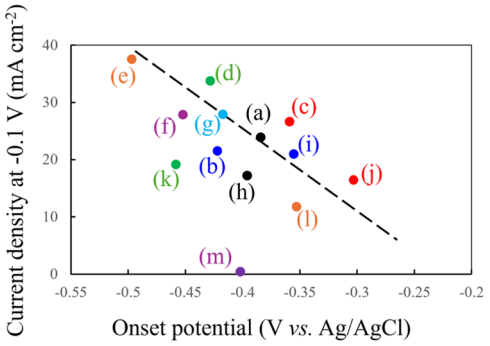

Figure 4. Plot of onset potential vs. current density at −0.1 V for MeOH oxidation on Pt NPs/CB (a) and Pt-based NPs/CB (b−m) in N_2-saturated 0.5 M MeOH and 0.1 M NaOH aqueous solutions at 10 mV s^{-1} and 2000 rpm.

$PtPb_{1.1}$/CB exhibited the highest current density of 37.5 mA cm^{-2} for MeOH oxidation. The trends of these results are similar to those we previously reported using bulk materials of Pt-based bimetallic alloys and intermetallic compounds.[12] Additionally, among the Pt-based NPs (B) used for EtOH oxidation, $PtPb_{1.1}$ showed the maximum activity of 33.0 mA cm^{-2}. The relationship between a smaller onset potential and a larger current density is clearly observed. A comparison of the results of the MeOH and EtOH oxidation reactions on the NPs revealed that the onset potential for EtOH oxidation was smaller. When the current density was observed at the same polarization magnitude as the onset potential, the magnitude of the current densities was equivalent for MeOH and EtOH oxidation.

The Pt-based NPs examined for MeOH and EtOH oxidation were subjected to XPS measurements to study the d-band center of Pt on the NP surfaces. The typical spectra of Pt in Pt-based NPs (a−d) used for evaluating the value of the d-band center are shown in Figure 5. The spectra for other NPs (e−m) are shown in Figure S5. The dotted line in Figures 5 and S5 is the baseline of the spectrum, and the area between the spectrum and the baseline is defined as the area of the spectrum. From the spectrum, the d-band center values of Pt on the Pt-based NPs were evaluated according to eq 1. In other words, in Figure 5, the d-band center value is the binding energy value on the line, which divides the area of the spectrum for the 5d orbital of Pt in half.

With the pair of current densities (Tables S1 and S2) and d-band centers of the NPs (Table S3), plots of the (A) MeOH and (B) EtOH oxidation catalytic activities *vs* the d-band center values were obtained (Figure 6). The plots show a volcano-type shape, as expected, for both MeOH and EtOH oxidation. The values of the current density and d-band center were averaged from three experiments. In the plots, the error bars of each data point are shown, and the maximum and minimum error bars are the maximum and minimum values among the three data points. The values of the d-band center showing maximum activities are −3.78 and −3.81 eV for MeOH and EtOH oxidation, respectively. The results of both MeOH and EtOH oxidation show that $PtPb_{1.1}$ is located near the maximum activity, which is in good agreement with the results reported thus far indicating that PtPb has high activity.[12,25,26] PtBi, which is located close to the maximum activity, is also well known as a highly active catalyst for MeOH and EtOH oxidation.[12,27,28]

Relationship between the Adsorbed Carbon Monoxide Oxidation Potential and the *d*-Band Center of Pt on the Pt-Based Catalyst Surfaces. The degree of adsorption of CO on Pt surfaces depends on the electronic

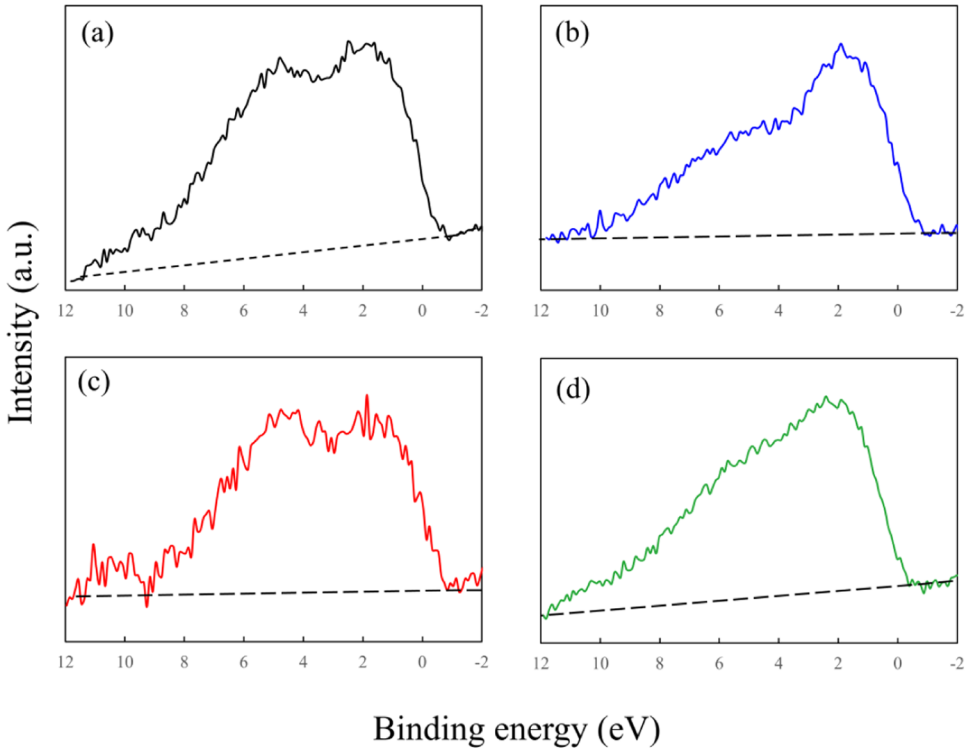

Figure 5. XPS profiles in the valence band region for Pt-based NPs/CB. (a) Pt/CB, (b) $PtRh_{0.5}$, (c) PtBi, and (d) $PtCo_{1.3}$. The area between the spectrum obtained and the baseline is used for the calculation of the d-band center.

https://doi.org/10.1021/acsomega.4c08380
ACS Omega 2025, 10, 10060−10070

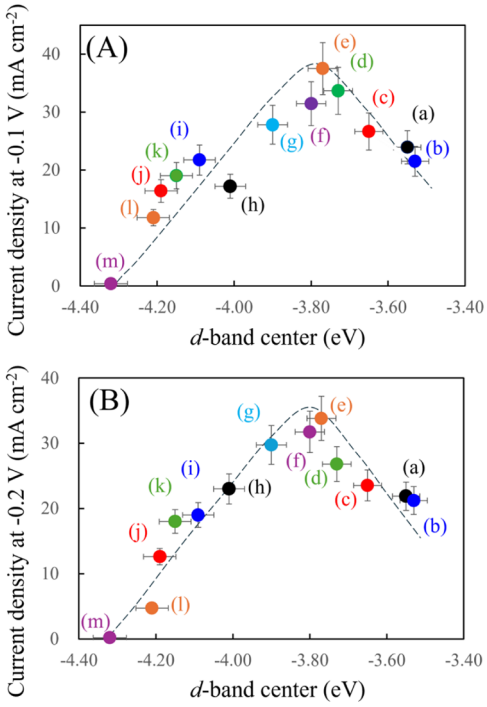

Figure 6. Relationship between the d-band centers of the Pt atoms in Pt NPs/CB (a) and Pt-based NPs/CB (b−m) and current density at −0.1 V ((A) MeOH oxidation) and −0.2 V ((B) EtOH oxidation).

state of Pt.[29] When CO molecules are adsorbed on Pt surfaces, the lowest antibonding molecular orbital (LUMO) $2\pi^*$ of CO hybridizes with the Pt-occupied 5d orbital. As a result, this hybridization induces a back-donation effect in which electrons transfer from Pt-5d to the $2\pi^*$ orbital of CO. This affects the adsorption strength of the adsorption of CO to Pt. In Pt-based NPs, if a second element in the NPs partially donates electrons to Pt, the highest energy level of the occupied electrons in the Pt-occupied 5d orbital increases and the electrons from Pt can fill more of the antibonding orbitals of CO, weakening the adsorption strength of CO to Pt. Zhang et al. detected this difference in CO adsorption strength from changes in the wavenumber of the infrared (IR) absorption peak related to CO in IR measurements.[29] In this study, the difference was detected electrochemically from the electrolytic oxidation potential of CO adsorbed on the Pt surface of Pt-based NPs. The potential of the CO oxidation peak differs depending on the degree of CO adsorption. Specifically, as the degree of CO adsorption decreases, the CO oxidation potential shifts more negatively.[30,31] The voltammograms for the oxidation of CO adsorbed on the Pt of the Pt-based NPs are shown in Figure S6. The oxidation potential of adsorbed CO was taken as the peak position of the CO oxidation.

Figure 7 shows the relationship between the oxidation potential of adsorbed CO and the value of the d-band center. In the $PtSn_{3.1}$(i), $PtSn_{3.3}$(j), and $PtSb_{1.4}$(m) samples, no CO was adsorbed on the NP surface, and no voltammograms for the oxidation of adsorbed CO were observed. Considering the electronic interaction between Pt and CO described above, it is expected that the oxidation potential of CO adsorbed on Pt will tend to move in the negative direction when the d-band center value is small (having a large negative value), and the plot in Figure 7 shows an approximate expected trend. The fact that the results showed the expected behavior means that the

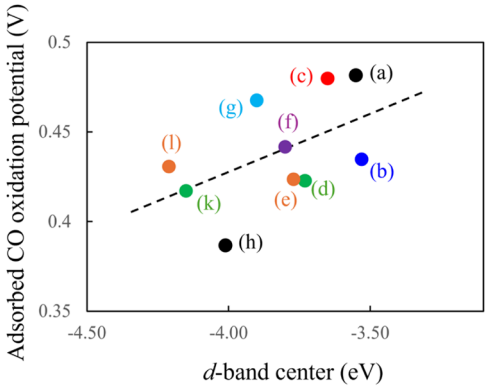

Figure 7. Relationships between the d-band centers of the Pt atoms in Pt NPs/CB (a) and Pt-based NPs/CB (b, c, d, e, f, g, h, k, and l) and the potential for CO adsorption and oxidation on the NP surfaces.

change in the electronic state of Pt in Pt-based NPs occurred, as predicted by the change in the second element in the NPs.

XAS Analysis of the Electronic State of Pt in Pt-Based NPs. As another method for evaluating the electronic state of Pt in the catalysts, XAS was applied to the NP samples to measure the vacancy in the 5d orbital of Pt in the NPs. In Figure 8, typical spectra of the Pt L_3 and L_2 edges in Pt-based NPs are shown. Another spectrum of the samples is shown in Figure S7. The vacancy of 5d orbitals was calculated by analyzing the spectra of the Pt L_3 and L_2 edges via eqs 2−4.[15] Figure S8 shows typical results of XAS spectrum of Pt on Pt NP/CB to evaluate the peak area. The vacancy values of the 5d orbitals for each sample are summarized in Table S4, and the relationships between the vacancy values of the 5d orbitals and the oxidation current densities of MeOH and EtOH are plotted in Figure 9. In contrast to the d-band center value mentioned above, when the second element partially donates an electron to Pt, the electron enters the Pt 5d orbital, reducing the degree of vacancy; therefore, the vacancy value decreases. The d-band center indicates the degree of filling of the d-orbital with electrons, and the vacancy degree of the d-orbital indicates the state in which the d-orbital is empty. In other words, they are looking at the state of the d-orbital electrons from the opposite direction. When based on the experimentally obtained d-band center values, the PtX NPs were arranged in order of the largest d-band center value they possess, and the order should be the same as the order of the PtX NPs arranged in order of the smallest vacancy degree of the d-orbital obtained in the experiment. When the PtX NPs used in this study are arranged from this perspective, the order of the d-band center and the order of the vacancy degree are the same, roughly as expected. Moreover, the plots of the Pt 5d orbital vacancy value vs current density for MeOH and EtOH oxidation also showed an approximate volcano-shaped plot similar to the plot of the d-band center. In Figure 9 (A), there is a large variability and it is difficult to make a definitive statement, but we have determined that the overall trend indicates volcanic behavior. The vacancy of the Pt 5d orbital at the maximum catalytic activity (maximum oxidation current density) estimated from the volcano-shaped plot was 0.369 for both MeOH and EtOH oxidation. This is consistent with the fact that the d-band center values plotted by using the d-band center values also showed that the optimal values of the d-band center showing maximum activity were almost the same for both MeOH and EtOH oxidation. These results confirmed

https://doi.org/10.1021/acsomega.4c08380
ACS Omega 2025, 10, 10060−10070

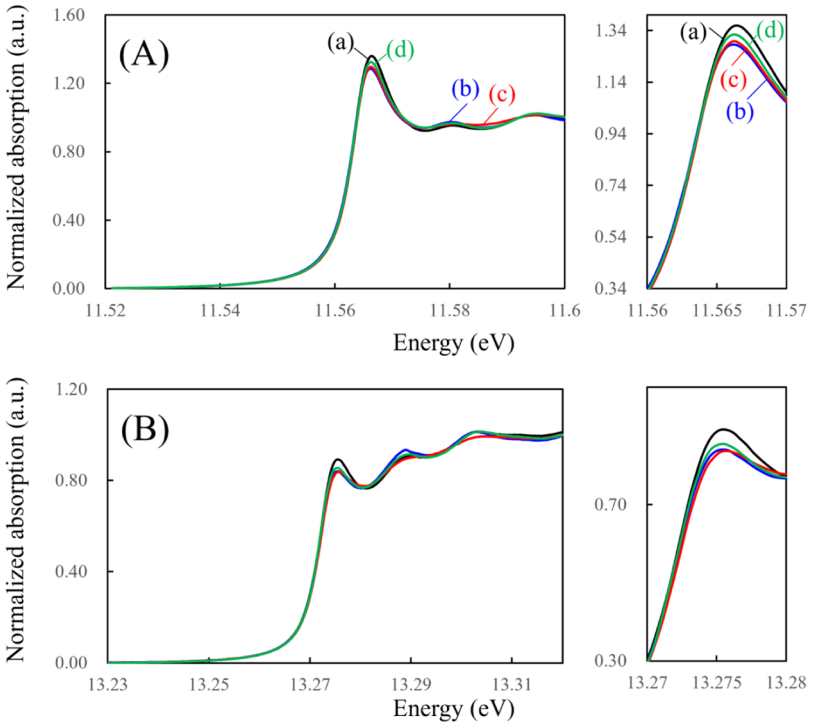

Figure 8. XAS profiles of the (A) L_3 and (B) L_2 edges of Pt for Pt-based NPs/CB. (a) Pt/CB, (b) $PtRh_{0.5}$, (c) PtBi, and (d) $PtCo_{1.3}$.

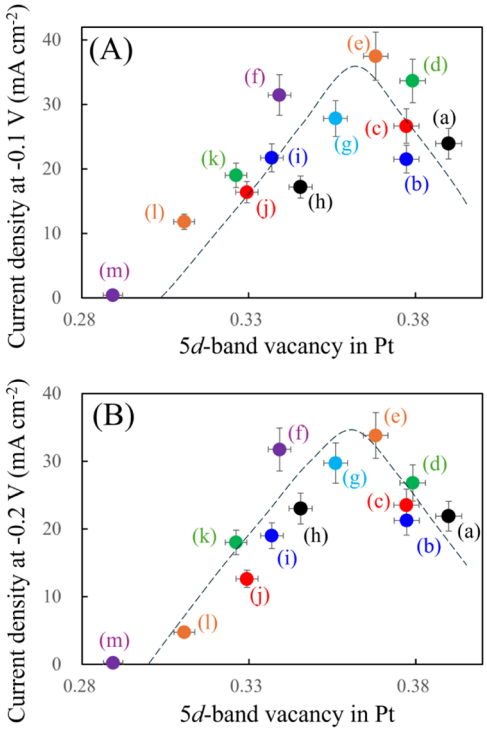

Figure 9. Relationships between the 5d-band vacancies of the Pt atoms in Pt NPs/CB (a) and Pt-based NPs/CB (b−m) and current density at −0.1 V ((A) MeOH oxidation) and −0.2 V ((B) EtOH oxidation).

that the electronic state of Pt and the catalytic activity exhibited the expected volcano-shaped relationship even when XAS measurements other than the XPS measurements examined thus far were used.

Relationship between the Electrochemical Activity and *d*-Band Center of Pt on Pt-Based Catalyst Surfaces in the Electrooxidation of Carbon-Containing Compounds. To confirm whether the volcano-shaped relationships observed in the oxidation reactions of MeOH and EtOH can also be observed in other oxidation reactions, a similar study was carried out for the oxidation reactions of formaldehyde and formate ions in alkaline aqueous solutions, which are thought to be intermediate products in the oxidation reactions of MeOH and EtOH. The voltammograms for these oxidation reactions are shown in Figures S9 and S10. Looking at the voltammograms obtained for each sample and each reaction, the potentials showing the maximum current density values vary, making comparisons difficult; however, here, the oxidation current density at −0.1 V, an indicator of catalytic activity, which is consistent with the MeOH oxidation reaction, was used.

The relationship between the Pt d-band center in the catalyst and catalytic activity is shown in Figure 10. For both oxidation reactions, the plots are volcano-shaped. For the oxidation of formaldehyde (A), a volcano-shaped plot is obtained, with the maximum activity current being slightly smaller than the maximum current for the oxidation of MeOH and EtOH. The major difference is that the Pt d-band center value showing the maximum activity is −3.90 eV, which is different from the values of −3.78 eV for MeOH and −3.81 eV for EtOH, indicating a change in the optimal d-band center value. Additionally, a second peak is observed at approximately −4.2 eV. In the oxidation reaction of formate ions (B), the value of the Pt d-band center showing maximum activity is −3.73 eV, which is slightly shifted compared with that of MeOH and EtOH. However, the oxidation current density decreases by more than one-sixth compared to the current density at the maximum activity for MeOH and EtOH oxidation. The results showed that almost no catalytic activity

https://doi.org/10.1021/acsomega.4c08380
ACS Omega 2025, 10, 10060−10070

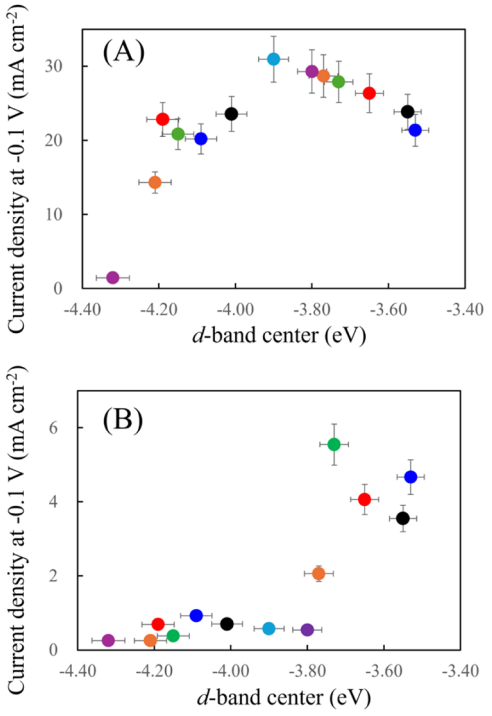

Figure 10. Relationship between the d-band center of the Pt atoms in Pt NPs/CB (a) and Pt-based NPs/CB (b−m) and current density for (A) formaldehyde and (B) formate oxidation reactions at −0.1 V in 0.1 M NaOH aqueous solutions containing 0.5 M formaldehyde or potassium formate at 10 mV s^{-1} and 2000 rpm.

was observed when the d-band center value was below −3.8 eV. It has been proposed that the oxidation pathway of MeOH involves the oxidation of MeOH to formaldehyde, which is then further oxidized to formate ions to produce carbon dioxide (CO_2).[32] The difference in the positions of the d-band center values that show maximum activity in these plots indicates that there is an optimal d-band center value for each elementary reaction when MeOH is oxidized to CO_2 and that this value must be adjusted. In the $PtPb_{1.1}$ sample, which showed the highest activity in MeOH oxidation, the product of the oxidation of MeOH was not CO_2 but mostly formate ions because formate ions could not be oxidized on the surface of the NPs. Furthermore, as shown by the volcano plot for the oxidation of formate ions, $PtPb_{1.1}$ showed the highest activity because NPs with d-band center values smaller than those of $PtPb_{1.1}$ could not oxidize formate ions; therefore, their activity began to decrease. In summary, as mentioned above, it is necessary to systematically evaluate the activity in each elementary reaction and the value of the Pt d-band center and to deeply consider the relationship between the reaction path and the d-band center value. In addition, it is necessary to analyze the products in each oxidation reaction, and information on how the products change, depending on the value of the d-band center, is also necessary for comprehensive consideration.

Volcano Plot of the Adatom-Modified Pt Surface. To evaluate the NP activity, electrochemical hydrogen adsorption measurements were used to measure the surface area of Pt on the NP surface. However, this method is applicable to pure Pt but is not considered applicable to Pt-based alloys. This is because the electronic state of Pt changes when Pt is alloyed with a second element, and as a result, the state of hydrogen adsorption also changes. To compare activities at more accurate current densities, the activity and d-band center values obtained using an adatom-modified electrode were evaluated. Adatom deposition occurs under the redox potential of metal ions on the basis of the interaction between the electrode surface and adatoms deposited below the layer level on the electrode surface.[21,33,34] Because the coverage of the Pt surface by adatom elements is low because of adatom deposition on the Pt surface, the electrode area used to calculate the current density was considered to be the surface area of the Pt electrode calculated by the adsorption of hydrogen atoms before adatom deposition. After the adatom deposition of the second element to the Pt electrode surfaces and the drying of the electrode surfaces, the d-band center values (Table S5) of the adatom-modified Pt electrode surfaces were evaluated *via* XPS measurements. The d-band center value of Pt on the Pt electrode was −3.17 eV. Moreover, the ratio of Pt to the second element on the adatom-modified electrode surface was determined *via* XPS measurements (Table S5). Voltammograms for MeOH on the adatom-modified Pt electrodes are shown in Figure S11. Compared with that of the Pt-based NPs, the onset potential is shifted significantly to the positive potential side, but the current curve after the oxidation current value increases is similar to that of the Pt-based NPs.

The relationships between the d-band center of Pt on the electrodes and the current density for MeOH oxidation on five types of adatom-modified electrodes, Pb, In, Cu, Co, and Bi adatom-modified Pt electrodes, and a Pt electrode were plotted (Figure 11). The plot is also a volcano plot. The d-band center

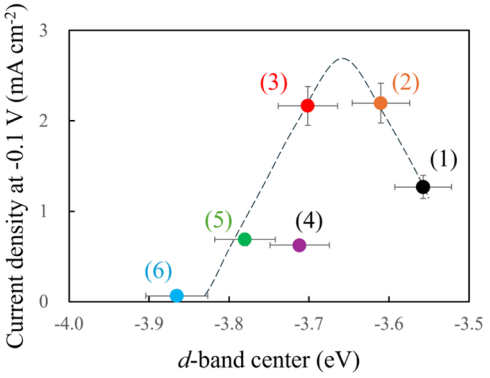

Figure 11. Relationships between the d-band centers of the Pt electrode (1), and Pb (2), Bi (3), In (4), Co (5), and Cu (6) adatom-modified Pt electrodes and current density for MeOH oxidation at −0.1 V.

value for the highest activity was −3.65 eV, which is significantly different from the optimal d-band center value of −3.8 eV obtained for Pt-based NPs, even though the same MeOH oxidation reaction was investigated. The reason for this difference is a problem with the value of the d-band center in the adatom-modified Pt electrode. In the case of adatom-modified Pt electrodes, the electronic state of Pt on the electrode surface changes due to electronic interactions between the adatom of the second element deposited on the Pt electrode surface and Pt, affecting the catalytic reaction; however, XPS measurements provide information about the electronic state of not only Pt on the electrode surface but also Pt, which is located close to the surface but inside and is not involved in this reaction. Since the information on Pt that is

https://doi.org/10.1021/acsomega.4c08380
ACS Omega 2025, 10, 10060−10070

not affected by the adatoms is also included, the value of the d-band center is believed to shift to the value of the Pt electrode. In conclusion, these results also confirmed that the catalytic activity of the MeOH oxidation reaction is affected by the electronic state of Pt and that there is an optimal electronic state. In this study, the electronic state of Pt in the catalyst was measured in the NP state. In reality, measurements are required while the electrochemical reaction is occurring. The electronic state may change when the catalyst comes into contact with electrolyte solutions. The electronic state may also change when intermediates generated during electrode reactions are adsorbed onto the catalyst surface. In fact, there is a paper that reports that the structure of the electrode surface changes when CO, which is generated as an intermediate in the oxidation reaction of MeOH and EtOH, used in this study, is adsorbed.[35] The electronic state may also change when the surface structure changes. Because of these various possibilities, we think that it is necessary to conduct research on the electronic state and electrocatalytic activity in situ in the future, and we are considering in situ XAS measurements.

CONCLUSIONS

In this study, the electrochemical oxidation of MeOH and EtOH on Pt-based NPs was used as the target reaction, and the aim was to clarify the relationship between the electronic state of the catalyst (the electronic state of Pt in the catalyst) and the catalytic activity. XPS and XAS measurements were used to evaluate the electronic state of the electrode catalyst. In addition, to confirm the change in the electronic state of Pt in the Pt-based NPs, the adsorption of CO onto the catalyst surfaces was investigated, and the relationship between the oxidation potential of adsorbed CO and catalytic activity was confirmed. The relationship between the electronic state of Pt in the catalyst and the catalytic activity shows a volcano-shaped trend, indicating that there is a suitable electronic state that maximizes the catalytic activity. Among the samples examined in this study, $PtPb_{1.1}$ showed the highest activity, which is thought to be due to its optimal electronic and atomic configuration. Strictly speaking, the XPS and XAS measurement results used in this study do not reflect the electronic state of the catalyst outermost surface. In this regard, we believe that measurement methods that can obtain information only from the surface should be applied to samples to obtain surface information. A careful look at the plots of the results reveals that there is another small peak in the volcano-shaped plot. The reason for this small peak is currently under investigation. We will investigate the reason for this in the future as it is believed to provide important information regarding the reaction mechanism and catalytic activity. In order to clarify the relationship between the structural factor of the catalyst and its catalytic activity in the analysis, the electronic state of surface atoms must be determined by using a single crystal with a regulated structure. It is also necessary to investigate the structure in more detail in conjunction with other measurements, and this is currently under consideration.

ASSOCIATED CONTENT

Supporting Information

The Supporting Information is available free of charge at https://pubs.acs.org/doi/10.1021/acsomega.4c08380.

Characterization and preparation of catalysts; experimental conditions of carbon monoxide-stripping voltammetry; TEM and HAADF-STEM images; electrochemical results; XPS profiles in the valence band region for Pt-based NPs/CB; XAS profiles of the L_3 and L_2 edges of Pt for Pt-based NPs/CB and summary of the data values of electrochemical experiments; and the d-band center value and Pt 5d orbital vacancy value (PDF)

AUTHOR INFORMATION

Corresponding Author

Futoshi Matsumoto − *Department of Applied Chemistry, Faculty of Chemistry and Biochemistry, Kanagawa University, Yokohama, Kanagawa 221-8686, Japan;* orcid.org/0000-0001-6808-6531; Email: fmatsumoto@kanagawa-u.ac.jp

Authors

Tamaki Matsumura − *Department of Applied Chemistry, Faculty of Chemistry and Biochemistry, Kanagawa University, Yokohama, Kanagawa 221-8686, Japan*

Mika Fukunishi − *Department of Applied Chemistry, Faculty of Chemistry and Biochemistry, Kanagawa University, Yokohama, Kanagawa 221-8686, Japan*

Complete contact information is available at: https://pubs.acs.org/10.1021/acsomega.4c08380

Author Contributions

T.M. and M.F. performed preparation, characterization, and electrochemical tests of samples. F.M. wrote the manuscript and summarized the work.

Notes

The authors declare no competing financial interest.

ACKNOWLEDGMENTS

A part of this work was supported by the "Advanced Research Infrastructure for Materials and Nanotechnology in Japan (ARIM)" of the Ministry of Education, Culture, Sports, Science and Technology (MEXT) Under proposal number 24KU0030. We are grateful to Dr. Y. Fukunaga at Kyushu University for her helpful support in the TEM-EDX analysis. This work was achieved under a proposal of Spring-8 (2023B1039, 2023B1944). The authors thank Dr. Kazuo Kato and Dr. Misaki Katayama for their valuable suggestions concerning XAFS and XANES measurements.

REFERENCES

(1) Peighambardoust, S. J.; Rowshanzamir, S.; Amjadi, M. Review of the proton exchange membranes for fuel cell applications. *Int. J. Hydrogen Energy* **2010**, *35*, 9349−9384.

(2) Jiao, K.; Xuan, J.; Du, Q.; Bao, Z.; Xie, B.; Wang, B.; Zhao, Y.; Fan, L.; Wang, H.; Hou, Z.; Huo, S.; Brandon, N. P.; Yin, Y.; Guiver, M. D. Designing the next generation of proton-exchange membrane fuel cells. *Nature* **2021**, *595*, 361−369.

(3) Alias, M. S.; Kamarudin, S. K.; Zainoodin, A. M.; Masdar, M. S. Active direct methanol fuel cell: An overview. *Int. J. Hydrogen Energy* **2020**, *45*, 19620−19641.

(4) Yaqoob, L.; Noor, T.; Iqbal, N. A comprehensive and critical review of the recent progress in electrocatalysts for the ethanol oxidation reaction. *RSC Adv.* **2021**, *11*, 16768−16804.

(5) An, L.; Chen, R. Direct formate fuel cells: A review. *J. Power Sources* **2016**, *320*, 127−139.

(6) Dumont, J. H.; Martinez, U.; Chung, H. T.; Zelenay, P. Ternary PtRuPd/C Catalyst for High-Performance, Low-Temperature Direct Dimethyl Ether Fuel Cells. *ChemElectroChem* **2016**, *3*, 1564−1569.

(7) Dillon, R.; Srinivasan, S.; Aricò, A. S.; Antonucci, V. International activities in DMFC R&D: status of technologies and potential applications. *J. Power Sources* **2004**, *127*, 112−126.
(8) Shaari, N.; Kamarudin, S. K.; Bahru, R.; Osman, S. H.; Ishak, N. A. I. M. Progress and challenges: Review for direct liquid fuel cell. *Int. J. Energy Res.* **2021**, *45*, 6644−6688.
(9) Chu, Y. H.; Shul, Y. G. Alcohol Crossover Behavior in Direct Alcohol Fuel Cells (DAFCs) System. *Fuel Cells* **2012**, *12*, 109−115.
(10) Pan, J.; Lu, S.; Li, Y.; Huang, A.; Zhuang, L.; Lu, J. High-Performance Alkaline Polymer Electrolyte for Fuel Cell Applications. *Adv. Funct. Mater.* **2010**, *20*, 312−319.
(11) Antolini, E.; Gonzalez, E. R. Alkaline direct alcohol fuel cells. *J. Power Sources* **2010**, *195*, 3431−3450.
(12) Matsumoto, F. Ethanol and methanol oxidation activity of PtPb, PtBi, and $PtBi_2$ intermetallic compounds in alkaline media. *Electrochemistry* **2012**, *80*, 132−138.
(13) Ando, F.; Gunji, T.; Tanabe, T.; Fukano, I.; Abruña, H. D.; Wu, J.; Ohsaka, T.; Matsumoto, F. Enhancement of oxygen reduction reaction activity of Pt by tuning its d-band center via transition metal oxide support interactions. *ACS Catal.* **2021**, *11*, 9317−9332.
(14) Ando, F.; Tanabe, T.; Gunji, T.; Kaneko, S.; Takeda, T.; Ohsaka, T.; Matsumoto, F. Effect of the d-band center on the oxygen reduction reaction activity of electrochemically dealloyed ordered intermetallic platinum-lead (PtPb) nanoparticles supported on TiO_2-deposited cup-stacked carbon nanotubes. *ACS Appl. Nano Mater.* **2018**, *1*, 2844−2850.
(15) Wang, X.; Orikasa, Y.; Uchimoto, Y. Platinum-based electrocatalysts for the oxygen-reduction reaction: determining the role of pure electronic charge transfer in electrocatalysis. *ACS Catal.* **2016**, *6*, 4195−4198.
(16) Lima, F. H. B.; Zhang, J.; Shao, M. H.; Sasaki, K.; Vukmirovic, M. B.; Ticianelli, E. A.; Adzic, R. R. Catalytic activity-*d*-band center correlation for the O_2 reduction reaction on platinum in alkaline solutions. *J. Phys. Chem. C* **2007**, *111*, 404−410.
(17) Wang, S.; Yang, F.; Jiang, S. P.; Chen, S.; Wang, X. Tuning the electrocatalytic activity of Pt nanoparticles on carbon nanotubes via surface functionalization. *Electrochem. Commun.* **2010**, *12*, 1646−1649.
(18) Tritsaris, G. A.; Nørskov, J. K.; Rossmeisl, J. Trends in oxygen reduction and methanol activation on transition metal chalcogenides. *Electrochim. Acta* **2011**, *56*, 9783−9788.
(19) Mansour, A. N.; Cook, J. W., Jr.; Sayers, D. E. Quantitative technique for the determination of the number of unoccupied d-electron states in a platinum catalyst using the $L_{2,3}$ X-ray absorption edge spectra. *J. Phys. Chem. A* **1984**, *88* (11), 2330−2334.
(20) https://bruceravel.github.io/home/.
(21) Chen, L.; Unocic, R. R.; Hoffman, A. S.; Hong, J.; Braga, A. H.; Bao, Z.; Bare, S. R.; Szanyi, J. Unlocking the catalytic potential of TiO_2-supported Pt single atoms for the reverse water−gas shift reaction by altering their chemical environment. *JACS Au* **2021**, *1*, 977−986.
(22) Matsumoto, F.; Uesugi, S.; Koura, N.; Okajima, T.; Ohsaka, T. Electrochemical reduction of molecular oxygen at Hg adatom-modified Au electrodes. *J. Electroanal. Chem.* **2001**, *505*, 150−158.
(23) Shao, M.; Odell, J. H.; Choi, S.-I.; Xia, Y. Electrochemical surface area measurements of platinum- and palladium-based nanoparticles. *Electrochem. Commun.* **2013**, *31*, 46−48.
(24) Zeng, J.; Han, M.; Lu, X.; Chen, D.; Liao, S. Highly ordered and surfactant-free Pt_xRu_y bimetallic nanocomposites synthesized by electrostatic self-assembly for methanol oxidation reaction. *Electrochim. Acta* **2013**, *112*, 431−438.
(25) Jiang, Q.; Jiang, L.; Qi, J.; Wang, S.; Sun, G. Experimental and density functional theory studies on PtPb/C bimetallic electrocatalysts for methanol electrooxidation reaction in alkaline media. *Electrochim. Acta* **2011**, *56*, 6431−6440.
(26) Wu, X.; Jiang, Y.; Yan, Y.; Li, X.; Luo, S.; Huang, J.; Li, J.; Shen, R.; Yang, D.; Zhang, H. Tuning surface structure of Pd_3Pb/Pt_nPb nanocrystals for boosting the methanol oxidation reaction. *Adv. Sci.* **2019**, *6*, No. 1902249.
(27) Wang, X.; Xie, M.; Lyu, F.; Yiu, Y.-M.; Wang, Z.; Chen, J.; Chang, L.-Y.; Xia, Y.; Zhong, Q.; Chu, M.; Yang, H.; Cheng, T.; Sham, T.-K.; Zhang, Q. Bismuth oxyhydroxide-Pt inverse interface for enhanced methanol electrooxidation performance. *Nano Lett.* **2020**, *20*, 7751−7759.
(28) Lu, Q.; Li, J.; Eid, K.; Gu, X.; Wan, Z.; Li, W.; Al-Hajri, R. S.; Abdullah, A. M. Facile one-step aqueous-phase synthesis of porous PtBi nanosponges for efficient electrochemical methanol oxidation with a high CO tolerance. *J. Electroanal. Chem.* **2022**, *916*, No. 116361.
(29) Zheng, J. H.; Li, G.; Zhang, J.-M.; Cheng, N.; Ji, L.-F.; Yang, J.; Zhang, J.; Zhang, B.-W.; Jiang, Y.-X.; Sun, S.-G. General strategy for evaluating the d-band center shift and ethanol oxidation reaction pathway towards Pt-Based electrocatalysts. *Sci. China Chem.* **2023**, *66*, 279−288.
(30) Guo, C.; Xia, S.; Tian, Y.; Li, F.; Xu, G.; Wu, F.; Niu, W. Probing local charge transfer processes of Pt−Au heterodimers in plasmon-enhanced electrochemistry by CO stripping techniques. *Phys. Chem. Chem. Phys.* **2024**, *26*, 5773−5777.
(31) Chen, S.; Liu, N.; Zhong, J.; Yang, R.; Yan, B.; Gan, L.; Yu, P.; Gui, X.; Yang, H.; Yu, D.; Zeng, Z.; Yang, G. Engineering support and distribution of palladium and tin on MXene with modulation of the d-band center for CO-resilient methanol oxidation. *Angew. Chem., Int. Ed.* **2022**, *61*, No. e202209693.
(32) Gojković, S. L. Mass transfer effect in electrochemical oxidation of methanol at platinum electrocatalysts. *J. Electroanal. Chem.* **2004**, *573*, 271−276.
(33) Bonilla, S. H.; Zinola, C. F.; Rodríguez, J.; Díaz, V.; Ohanian, V. D. M.; Ohanian, M.; Martínez, S.; Giannetti, B. F. Catalityc effects of ruthenium and osmium spontaneous deposition on platinum surfaces toward methanol oxidation. *J. Colloid Interface Sci.* **2005**, *288*, 377−386.
(34) Atkinson, R. W., III; John, S. S.; Dyck, O.; Unocic, K. A.; Unocic, R. R.; Burke, C. S.; Cisco, J. W.; Rice, C. A.; Zawodzinski, T. A., Jr.; Papandrew, A. B. Supportless, bismuth-modified palladium nanotubes with improved activity and stability for formic acid oxidation. *ACS Catal.* **2015**, *5*, 5154−5163.
(35) Tao, F.; Dag, S.; Wang, L.-W.; Liu, Z.; Butcher, D. R.; Bluhm, H.; Salmeron, M.; Somorjai, G. A. Break-up of stepped platinum catalyst surfaces by high CO coverage. *Science* **2010**, *327*, 850−853.

https://doi.org/10.1021/acsomega.4c08380
ACS Omega 2025, 10, 10060−10070